Original Article

Molecular screening of phytocompounds targeting the interface between influenza A NS1 and TRIM25 to enhance host immune responses

Muhammad Suleman [a,b], Abrar Mohammad Sayaf [c], Abbas Khan [d],
Salman Ali Khan [e], Norah A. Albekairi [f], Abdulrahman Alshammari [f],
Abdelali Agouni [d,*], Hadi M. Yassine [g,h,**], Sergio Crovella [a,*]

[a] Laboratory of Animal Research Center (LARC), Qatar University, Doha, Qatar
[b] Center for Biotechnology and Microbiology, University of Swat, Swat, Pakistan
[c] School of Chemical Sciences, Universiti Sains Malaysia, Gelugor, Penang, Malaysia
[d] Department of Pharmaceutical Sciences, College of Pharmacy, QU Health, Qatar University, P.O. Box 2713, Doha, Qatar
[e] Tunneling Group, Biotechnology Centre, Doctoral School, Silesian University of Technology, Akademicka 2, 44-100 Gliwice, Poland
[f] Department of Pharmacology and Toxicology, College of Pharmacy, King Saud University, Post Box 2455, Riyadh 11451, Saudi Arabia
[g] Biomedical Research Center, Qatar University, 2713 Doha, Qatar
[h] College of Health Sciences-QU Health, Qatar University, 2713 Doha, Qatar

ARTICLE INFO

ABSTRACT

Background: Influenza A virus causes severe respiratory illnesses, especially in developing nations where most child deaths under 5 occur due to lower respiratory tract infections. The RIG-I protein acts as a sensor for viral dsRNA, triggering interferon production through K63-linked poly-ubiquitin chains synthesized by TRIM25. However, the influenza A virus's NS1 protein hinders this process by binding to TRIM25, disrupting its association with RIG-I and preventing downstream interferon signalling, contributing to the virus's evasion of the immune response.

Methods: In our study we used structural-based drug designing, molecular simulation, and binding free energy approaches to identify the potent phytocompounds from various natural product databases (> 100,000 compounds) able to inhibit the binding of NS1 with the TRIM25.

Results: The molecular screening identified EA-8411902 and EA-19951545 from East African Natural Products Database, NA-390261 and NA-71 from North African Natural Products Database, SA-65230 and SA-4477104 from South African Natural Compounds Database, NEA- 361 and NEA- 4524784 from North-East African Natural Products Database, TCM-4444713 and TCM-6056 from Traditional Chinese Medicines Database as top hits. The molecular docking and binding free energies results revealed that these compounds have high affinity with the specific active site residues (Leu95, Ser99, and Tyr89) involved in the interaction with TRIM25. Additionally, analysis of structural dynamics, binding free energy, and dissociation constants demonstrates a notably stronger binding affinity of these compounds with the NS1 protein. Moreover, all selected compounds exhibit exceptional ADMET properties, including high water solubility, gastrointestinal absorption, and an absence of hepatotoxicity, while adhering to Lipinski's rule.

Conclusion: Our molecular simulation findings highlight that the identified compounds demonstrate high affinity for specific active site residues involved in the NS1-TRIM25 interaction, exhibit exceptional ADMET properties, and adhere to drug-likeness criteria, thus presenting promising candidates for further development as antiviral agents against influenza A virus infections.

* Corresponding authors.
** Corresponding author at: Biomedical Research Center, Qatar University, 2713 Doha, Qatar.
E-mail addresses: suleman@uswat.edu.pk (M. Suleman), amsayaf@gmail.com (A.M. Sayaf), abbas.khan@qu.edu.qa (A. Khan), salman.ali@polsl.pl (S.A. Khan), nalbekairi@ksu.edu.sa (N.A. Albekairi), abdshammari@ksu.edu.sa (A. Alshammari), aagouni@qu.edu.qa (A. Agouni), hyassine@qu.edu.qa (H.M. Yassine), sgrovella@qu.edu.qa (S. Crovella).

Introduction

Influenza A virus (IAV) is a major cause of respiratory infections that can lead to severe complications and even death [1]. According to the World Health Organization (WHO), there are around a billion cases of seasonal influenza annually, including 3–5 million cases of severe illness [2]. It causes 145,000 respiratory deaths annually [3]. Ninety-nine percent of deaths in children under 5 years of age with influenza-related lower respiratory tract infections are in developing countries [4]. In addition, Influenza A presents the potential for pandemics, which may arise with the emergence of a new subtype of the influenza virus or when an influenza virus from animals crosses species and starts spreading among humans. [5]. The 2009 pandemic alone is estimated to have caused 100,000–400,000 deaths, not only among groups considered to be at a higher risk of complications, such as the elderly, persons with chronic conditions and pregnant women, but also in young, healthy individuals [2]. Influenza epidemics and pandemics cause significant morbidity and mortality, costs to health services and economic losses due to work absenteeism [6]. Therefore, understanding the molecular mechanisms of IAV infection and immune evasion is crucial for developing effective prevention and treatment strategies, also with positive impact for society and economics [7].

Recognition of viral pathogens infecting host cells is detected by pattern recognition receptors (PRRs), such as RIG-I, belonging to the RIG-I-like receptor (RLR) family of PRRs. These receptors typically remain in an inactive state within uninfected cells, where the N-terminal tandem CARDs (caspase activation and recruitment domains) are inaccessible for signalling [8,9]. Upon activation, RIG-I sets off a signaling cascade dependent on TRIM25 E3 ligase activity, triggering the production of IFNs (interferons) and inflammatory cytokines. Viral RNA interaction along with ATP binding disrupts RIG-I's autoinhibited state, permitting TRIM25 to facilitate K63-linked polyubiquitination of its second CARD [10,11]. This ubiquitination, in turn, promotes RIG-I's assembly into a helical structure, enabling its interaction with the downstream effector MAVS (mitochondrial antiviral signaling protein). MAVS functions as a crucial link between RIG-I and various proteins and enzymes responsible for activating IRF3 and NF-κB, pivotal factors controlling the expression of genes encoding IFN-α and IFN-β [12]. These genes are responsible for producing proteins secreted by the cell, binding to receptors present in the same or neighbouring cells [13,14]. On the flip side, certain research findings highlight RIPLET as a crucial E3 ligase in antiviral defense, enhancing the antiviral signaling capabilities of the viral RNA receptor RIG-I through both Ub-dependent and independent pathways. Utilizing its dimeric configuration and a bivalent binding mechanism, RIPLET exhibits a preference for identifying and ubiquitinating RIG-I that is pre-oligomerized on double-stranded RNA [15–17].

Pathogenic viruses have developed various strategies to hijack the RIG-I signaling pathway, thus suppressing the host's innate immune response [18,19]. One such instance is observed in the non-structural protein 1 (NS1) of influenza A viruses (IAV). NS1 serves as a multifunctional virulence factor that interacts with numerous host proteins upon infection, including TRIM25 [20]. Structurally, NS1 consists of an RNA-binding domain (RBD, amino acids 1–73), connected by a short linker to the effector domain (ED, amino acids 85–202), followed by an unstructured C-terminal tail. Detailed studies involving the individual domains and complete structures of NS1 have shed light on NS1's self-association, the flexible nature of RBD and ED architecture, and its interactions with double-stranded RNA (dsRNA) and host proteins [21,22]. NS1 forms a constitutive homodimer by strongly interacting between its RBDs, while it can assemble into higher-order oligomers based on concentration levels due to weaker interactions among its EDs involving the surface area, notably featuring W187. These higher-order structures might be essential for specific functions like binding to double-stranded RNA [23]. However, the NS1 of the influenza A virus can bind to TRIM25's

coiled-coil domain, thereby disrupting its interaction with RIG-I. Consequently, this inhibition prevents RIG-I ubiquitination and subsequent downstream signaling [24]. Several small molecule inhibitors of NS1-ED have been reported in the literature, such as A9, A22, and JJ3297, which bind to a hydrophobic pocket in the ED and disrupt its interaction with CPSF30 [25]. These compounds have shown antiviral activity against different strains of IAV in-vitro and in-vivo. However, they showed some limitations, such as low potency, poor bioavailability, or high toxicity [26]. Moreover, the emergence of drug-resistant mutants poses a challenge for the development of effective NS1-ED inhibitors.

Natural products (NPs) are a rich source of chemical diversity and biological activity, and have been widely used as drugs or lead compounds for various diseases [27–29]. NPs have also shown potential as anti-IAV agents, either by directly inhibiting viral proteins or by modulating the host immune system [30]. However, the identification of NPs that target NS1-ED is still scarce and requires extensive screening and validation [31]. To overcome this challenge, we employed a computational approach that combines molecular docking and molecular dynamics (MD) simulations to screen a large collection of NPs from different databases against the NS1-ED binding interface [32,33]. Molecular docking is a fast and efficient method to predict the binding modes and affinities of ligands to a receptor [34]. Though, docking often neglects the receptor flexibility and the dynamic nature of protein-ligand interactions, which may affect the accuracy and reliability of the results [35]. Therefore, we integrated MD simulations with docking to refine the binding poses, evaluate the stability and interactions of the complexes, and calculate more realistic binding free energies [36]. To inhibit the binding of NS1 with the TRIM25, we screened NPs from various databases, such as Chinese Medicines Database (TCM), North African Natural Products Database (NANPDB), East African Natural Products Database (EANPDB), and North-East African Natural Products Database (ANPDB) and the South African Natural Compounds Database (SANCDB). These databases contain NPs from diverse sources, such as plants, animals, fungi, bacteria, or marine organisms, with different chemical structures and biological activities [37].

In this article, we present the results of our computational screening of NPs against NS1-ED using docking and MD simulations. We identified several NPs that showed high binding affinity and stability to NS1-ED, as well as favourable interactions with E95 and E96 residues which were previously identified as important binding residues. Furthermore, we juxtaposed our findings with those achieved through standalone docking or employing distinct scoring functions. We explore the strengths and limitations of our methodology, along with its potential implications for drug discovery and development against IAV infection.

Materials and methods

Crystal structure retrieval and preparation

The complex crystal structure of NS1-ED in complex with TRIM25 coiled-coil domain (PDB ID: 5NT1) was obtained from Research Collaboratory for Structural Bioinformatics, Protein Data Bank (RCSB, PDB) [24] (https://www.rcsb.org/structure/5nt1). The complex structure was then subjected to PyMOL for the removal of water molecules [38]. The addition of hydrogen atoms and minimization of the protein structure was achieved by using Chimera [39,40].

Molecular screening of natural products libraries

The drug repositories, such as the Traditional Chinese Medicines Database (TCM), North African Natural Products Database (NANPDB), East African Natural Products Database (EANPDB), North-East

African Natural Products Database (ANPDB), and South African Natural Compounds Database (SANCDB), were obtained and processed to ensure they met the required format. These collections contain diverse natural products from South Africa and China, each possessing various medicinal properties. To eliminate compounds that breach Lipinski's rule of five (R5) and are potentially toxic, the databases underwent screening using the FAF4drug online webserver [40]. Before employing EasyDock Vina 2.0 for virtual drug screening, the drugs underwent conversion into.pdbqt format. The Ligands' preparation involved generating the pdbqt format, where tools like Open Babel were utilized to assign atomic charges and atom types. The non-polar hydrogen atoms, Gasteiger charges, and torsion tree roots for flexibility analysis were considered in the ligand's preparation process. In contrast, the receptor necessitated preparation as grid maps within AutoGrid to delineate the docking space. This encompassed configuring grid dimensions, spacing, and specifying the macromolecule in pdbqt format, which entailed the addition of hydrogen atoms, charges, and atom types. Furthermore, the receptor grid was established based on the crystal structure of the NS1-TRIM25 complex. This software offers a user-friendly graphical interface for screening virtual databases. The AUTODOCK4 algorithm was utilized in the screening process to evaluate and prioritize potential drug candidates. Initially, a lower exhaustiveness setting of 16 was chosen for rapid preliminary screening. Following this, the most promising compounds, based on their scores, underwent a second screening with a higher exhaustiveness value of 64. This step was aimed at eliminating false positives and re-evaluating the top-ranking compounds. Subsequently, from each database, the top-ranking 10% of drugs identified in the previous process underwent induced-fit docking (IFD) using AutoDockFR. AutoDockFR typically employs force fields such as Amber or CHARMM, simulation protocols like molecular dynamics (MD), and scoring functions such as Amber scoring or force-field-based scoring for IFD simulations. The default parameters for the IFD docking were utilized. This method accommodates receptor flexibility and enables covalent docking [41]. Finally, the top two hits from each database were subjected to visual analysis using PyMOL and Schrodinger Maestro (free academic version for visualization) and molecular simulation for further validations [42].

Molecular simulation of top-scoring hits

To perform the MD simulation, all the coordinate and topology files for each complex were prepared by using the "tLeap" module within Amber21 [43,44]. Amber21 is a cutting-edge molecular dynamics simulation software, boasting advanced algorithms and enhanced performance capabilities. Designed for precision and efficiency, it offers researchers unparalleled control and insight into complex biomolecular systems. Each system was enclosed in a solvent box (Optimal Point Charge, OPC), and ions were inserted to neutralize charges. Parameterization of the ligand molecule utilized the GAFF2 force field, generating initial topology and frcmod files via antechamber and parmchk2. Following this, energy minimization was performed using algorithms like steepest descent and conjugate gradient. The minimization process iterated until specific convergence criteria, such as reaching a maximum force or meeting an energy change threshold, were achieved. Utilizing a temperature coupling algorithm, like Langevin Dynamics or Berendsen thermostat, each system underwent a gradual temperature increase for equilibration to reach the desired simulation temperature. The calculation of long-range electrostatic interactions relied on the Particle Mesh Ewald (PME) method, while van der Waals forces were determined using Lennard-Jones potential [45]. The equilibration process involved multiple stages, including positional restraint, gradual heating, and subsequent unrestrained equilibration, at the target temperature and pressure. To preserve covalent bond lengths

and angles, the SHAKE algorithm was applied. Pressure control was maintained using a barostat such as Berendsen or Andersen [46]. Following equilibration, a production simulation of 300 ns was conducted for each system using a molecular dynamics algorithm, either under NPT or NVT ensemble conditions [47].

Post-simulation analysis of the top hits-NS1 complexes

The resulting trajectory from simulation production was analyzed using CPPTRAJ or PTRAJ modules [48], wherein several key metrics such as RMSD, RMSF, SASA, and hydrogen bonding were calculated for each system [49–51]. RMSD, which quantifies the variance between the original and superimposed structures, is determined using the following mathematical equation:

$$RMSD = \sqrt{\frac{\sum d^2 i = 1}{N_{atoms}}} \tag{1}$$

Here, 'di' denotes the positional variance between atoms, while 'i' refers to both the original and superimposed structures. Additionally, the evaluation of the Root Mean Square Fluctuation (RMSF) involves utilizing the B-factor to measure the flexibility of individual protein residues. Mathematically, RMSF is determined as follows:

$$Thermal\ factor\ orB - factor = [(8\pi^{**}2)/3]\,(msf) \tag{2}$$

Binding free energy and dissociation constant (KD) analysis

The end-point total binding free energy was estimated by using the Molecular Mechanics Generalized Born Surface Area (MM/GBSA) method, which is a widely used and reliable approach for evaluating the binding affinity of protein-ligand complexes [42]. Using the MMPBSA.py script, the stable frames from the simulation trajectories were selected for free energy calculations [40]. The total binding free energy was computed as the difference between the free energy of the complex and the sum of the free energies of the protein and the ligand, as shown in the following equation [52]:

$$\Delta Gbind = \Delta Gcomplex - (\Delta Greceptor + \Delta Gligand) \tag{3}$$

The free energy of each component was calculated as the sum of several energy terms, including bonded, electrostatic, van der Waals, polar and non-polar contributions, as shown in the following equation [52]:

$$G = Gbond + Gelectrostatic + GvdW + Gpolar + Gnon - polar \tag{4}$$

The bonded term represents the interactions among covalently bonded atoms, such as bond stretching, angle bending and torsion. The electrostatic and van der Waals terms represent the Coulombic and dispersion forces between non-bonded atoms, respectively [53]. The polar and non-polar terms represent the solvation effects of the solvent on the solute, which depend on the solvent dielectric constant and the solute accessible surface area [42,54]. The polar term was estimated using the generalized Born (GB) model, which approximates the polar solvation energy by a pairwise interaction potential based on the effective Born radii of the atoms. The non-polar term was estimated using a linear combination of the solvent-accessible surface area (SASA) and a constant offset [40]. This free energy calculation method has been successfully applied by various studies to investigate the binding affinity and selectivity of different ligands against different targets [55,56]. Furthermore, the dissociation constant (KD) for the top hits was computationally predicted by using PRODIGY-LIGAND web servers. This server was previously used to predict the KD of different molecules used against different diseases [53].

Lipinski's rule, and pharmacokinetics analysis

Lipinski's Rule of Five serves as a fundamental guideline in drug design, emphasizing that successful orally administered drugs tend to have molecular properties within specific ranges: molecular weight < 500, hydrogen bond donors ≤ 5, hydrogen bond acceptors ≤ 10, octanol-water partition coefficient (logP) ≤ 5. This rule aids in predicting a compound's oral bioavailability and permeability, optimizing drug-like characteristics for effective pharmaceutical development [57]. To analyze **Lipinski's** rule of five, we used the online server SwissADME (http://www.swissadme.ch/) [58]. ADMET, encompassing Absorption, Distribution, Metabolism, Excretion, and Toxicity, constitutes crucial pharmacological traits evaluated for each drug candidate. The success of drug development heavily relies on these characteristics, with approximately 50% of drugs failing due to non-compliance with these fundamental pharmacokinetic principles [59]. To assess these attributes, in silico ADMET studies were conducted utilizing an online web tool server named pkCSM (https://biosig.lab.uq.edu.au/pkcsm/) [60]. Various pharmacokinetic parameters such as water solubility, coca-2 permeability, human intestinal absorption, blood-brain barrier (BBB) penetration, cytochrome P450 inhibition and substrate, AMES toxicity, skin sensitization, and hepatotoxicity levels were computed for the selected top hits natural compounds.

Results and discussion

The ability of the influenza A virus non-structural protein 1 (NS1) to interact with the coiled-coil domain of TRIM25 interrupts its association with RIG-I. This interference hampers RIG-I ubiquitination, impeding the subsequent immune system activation signaling [24]. To prevent NS1 from binding with TRIM25, we explored natural product databases for inhibitors targeting NS1-ED interaction. The TCM database covers 499 Chinese herbs with 29,384 ingredients, 3311 targets and 837 associated diseases, some of which became drugs like artemisinin [61]. ANPDB has 1012 compounds from African plants and marine life, some of which showed activity against microbes, cancer, diabetes, and neurological disorders [62]. SANCDB has 600 compounds from South African flora and fauna, some of which showed activity against HIV, tuberculosis, malaria, and cancer [62]. We focused on the residues Leu95, Ser99, Asn133, Tyr89, Thr91, Met93, and Asp92 of NS1-ED, which are involved in the interaction with TRIM25. We selected the top 10 compounds with the lowest docking scores and analyzed their interactions with NS1-ED summarized in **Table:1**. The most common functional groups that form hydrogen bonds are the hydroxyl groups (OH) of the phenolic compounds, such as catechol, pyrogallol, carboxylic acid, and chromene. The most common amino acids that form hydrogen bonds are Leu95, Ser99, Asn133, and Tyr89 of NS1-ED, which are key residues for the inhibition of NS1-TRIM25 binding. The distances of the hydrogen bonds range from 1.67 to 2.67 Å, which indicates strong and stable interactions. The unique functional group that forms a π-π interaction is the benzene ring of the anthraquinone compound alizarin, which interacts with Tyr89 of NS1-ED.

Top hits from East Africa natural product database

In East African natural database, we found two compounds, (-)-mesquitol and 5,7,3′,4′-tetrahydroxyflavanol, that showed binding affinity to NS1-ED, with docking scores of − 5.946 kcal/mol and − 5.689 kcal/mol, respectively. (-)-Mesquitol is a phenolic compound isolated from the bark of Prosopis juliflora, a plant with anti-inflammatory and antioxidant properties [63]. 5,7,3′,4′-tetrahydroxyflavanol is a flavonoid compound found in the leaves of Erythrina abyssinica, a plant with antimalarial and antimicrobial activity[64]. The hydroxyl groups (OH) of the catechol and chromene rings of these compounds acted as hydrogen bond donors or acceptors, and the distances of the hydrogen bonds ranged from 1.67 to 2.67 Å (Fig. 1). (-)-mesquitol formed five hydrogen bonds via hydroxyl group of
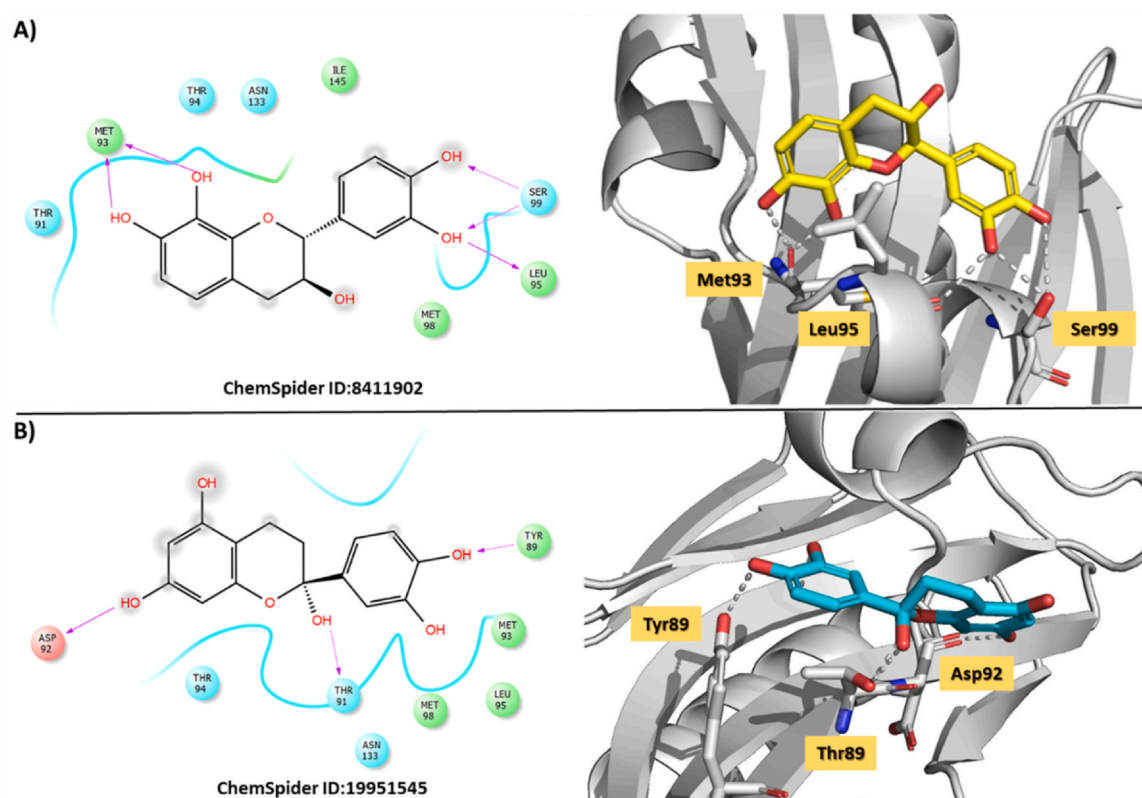
Fig. 1. Interaction pattern of top two hits from EANPD database with NS1 (**a**) showing the 2D and 3D interaction of top hit 1-NS1 complex (**b**) showing the 2D and 3D interaction of top hit 2-NS1 complex.
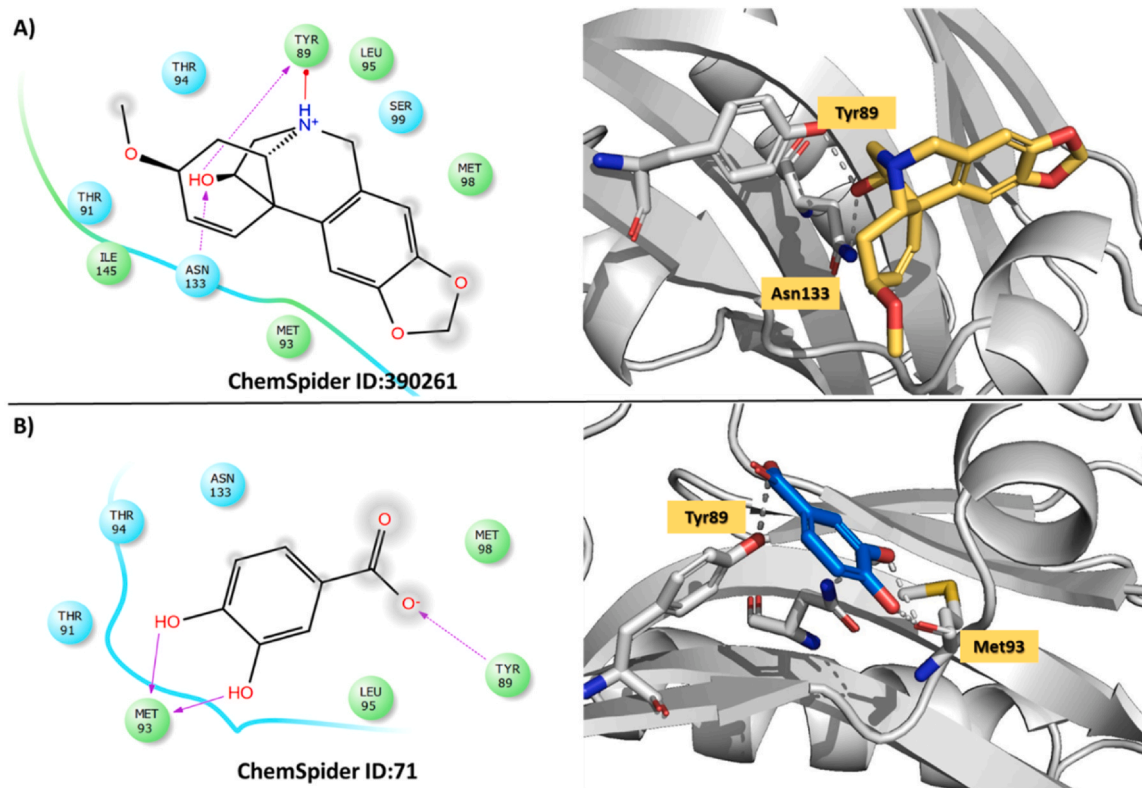
Fig. 2. Interaction pattern of top two hits from NANPDB database with NS1 (**a**) showing the 2D and 3D interaction of top hit 1-NS1 complex (**b**) showing the 2D and 3D interaction of top hit 2-NS1 complex.

chroman and catechol with Met93, Ser99 and Leu95 of NS1-ED (Fig. 1**a**). While second top hit, 5,7,3′,4′-tetrahydroxyflavanol formed three hydrogen bonds with Tyr89, Thr91, and Asp92 through hydroxyl groups of respective oxane/resorcinol/catechol ring with NS1-ED (Fig. 2**a**). These hydrogen bonds could affect the structural integrity and flexibility of NS1-ED, its binding with the TRIM25 which involve in the host immune evasion mechanism.

Top hits from North Africa natural product database

Haemanthamine and protocatechuic acid compounds were shortlisted from NANPDB, with a docking score of − 6.730 kcal/mol and − 5.71 kcal/mol, respectively. Haemanthamine is an alkaloid compound derived from the bulbs of Haemanthus multiflorus, a plant whose extracts have been already reported to possess some anticancer and antiviral activity [65]. Protocatechuic acid is a phenolic compound obtained from the fruits of Ziziphus lotus, a plant with antioxidant and anti-inflammatory activity [66]. The carboxylate (COOH), hydroxyl (OH) and ammonium (NH) group of these compounds acted as hydrogen bond donors or acceptors, hence extending hydrogen bonds ranging from 1.67 to 2.67 Å (Fig. 2). The hydroxyl group of Azabicyclooctanium of Haemanthamine and protocatechuic acid formed hydrogen bonds with Tyr89 of NS1-ED, which is a critical residue for the NS1-TRIM25 binding. Moreover, haemanthamine also formed a hydrogen bonds from azabicyclooctanium with Asn133, while protocatechuic acid formed two hydrogen bonds with Met93 of NS1-ED from hydroxyl groups of carboxylate functional group (Fig. 2**a & b**). These interactions indicate that these compounds could disrupt the NS1-TRIM25 binding interface.
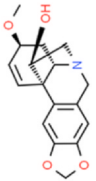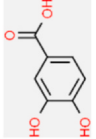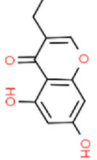
Top hit from the South Africa natural product database

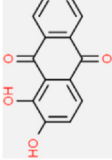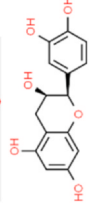Screening of SANPDB identified two top-scoring compounds (-)-epicatechin and isoeugenitol, showing docking scores of − 6.356 kcal/mol and − 5.96 kcal/mol. (-)-Epicatechin is a flavonoid

compound found in the bark of Acacia mearnsii, a plant with anti-diabetic and antioxidant activity [67]. Isoeugenitol is a phenolic compound derived from the leaves of Eugenia uniflora, a plant with antiviral and antibacterial activity [68]. The functionalities chromene, tetrahydropyran, catechol and pyranone group present in both compounds act as hydrogen bond donors or acceptors forming hydrogen bonds ranging from 1.67 to 2.67 Å (Table 1). Both compounds formed hydrogen bonds from resorcinol hydroxyl group with Ser99 and Leu95 of NS1-ED, which are essential residues for the NS1-TRIM25 binding. Furthermore, (-)-epicatechin formed hydrogen bonds with Tyr89 and Asn133 also from Oxane ring 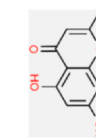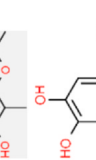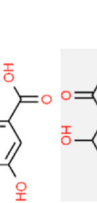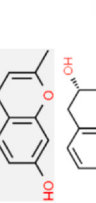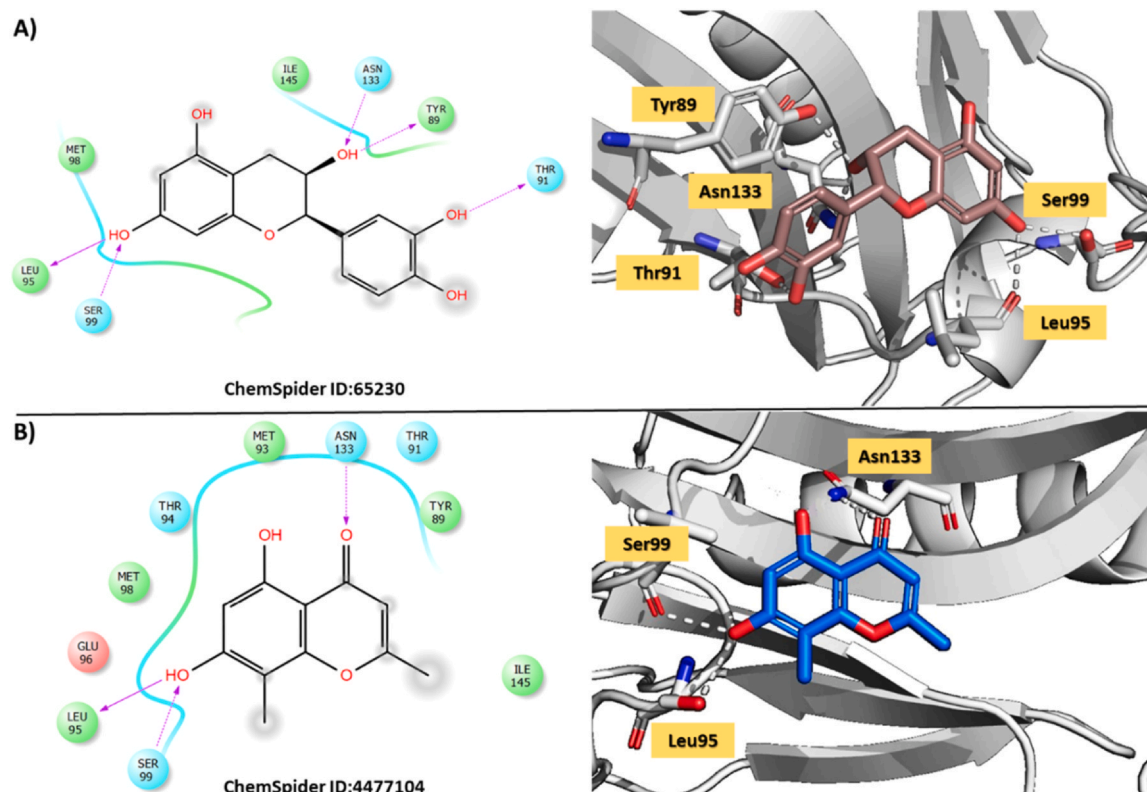while isoeugenitol form hydrogen bonding from carbonyl oxygen of pyranone ring. The hydroxyl group of catechol ring also engaged Thr91 (Fig. 3**a & b**). These interactions suggest that these compounds could inhibit the NS1-TRIM25 binding interface.

Top hit From the North East Africa natural product database

On the basis of specific bonding network and high docking scores we selected two top hits compounds from NENPDB, gallic acid and 5,7-dihydroxy-2-methylchromone, that displayed a docking score of − 5.099 kcal/mol and − 6.042 kcal/mol respectively. Gallic acid is a phenolic compound isolated from the leaves of Terminalia chebula, a plant with antiviral and immunomodulatory activity [69]. 5,7-dihydroxy-2-methylchromone is a chromone compound extracted from the roots of Oroxylum indicum, a plant with anticancer and anti-inflammatory activity [70]. Both compounds formed hydrogen bonds with key residue, Leu95 of NS1-ED, which is a vital residue for the NS1-TRIM25 binding. Additionally, gallic acid formed two hydrogen bonds with Thr94 and Thr91 through pyrogallol hydroxyl group, while 5,7-dihydroxy-2-methylchromone formed a hydrogen bond via carbonyl group of chromone ring with Thr89 of NS1-ED (Fig. 4**a & b**). These interactions imply that these compounds could block the NS1-TRIM25 binding interface.

Table 1

List of the top hits compounds with their Databases, IDs, 2D structures, scientific names, docking scores, interacting residues, bond distances, and interaction types. (Hydrogen bonding: HB and pi pi interaction: π-π).

2D Structure ChemSpider ID	Database, Common Name IUPAC Name	Docking score	Functional group	Interaction Nature	Interacting residues	Interaction Distance/Å
	NANPDB, Haemanthamine (3β,11 R,13β,19α)- 3-Methoxy 1,2 didehydrocrinan-11-ol	-6.730 kcal/mol	NH(Azabicycloctanium)	HB	Tyr89	1.74
			OH (Azabicycloctanium)	HB	Asn133	1.93
			NH(Azabicycloctanium)	π-cation	Tyr389	5.69
	NANPDB, Protocatechuic acid, 3,4dihydroxybenzoic acid	-5.71 kcal/mol	OH(carboxylate)	HB	Tyr89	2.17
			OH(catechol)	HB	Met93	1.72
			OH(catechol)	HB	Met93	1.94
	TCM, Lathodoratin, 3-ethyl-5,7-dihydroxychromen-4-one	-6.001 kcal/mol	CO(Pyranone)	HB	Meth93	2.07
			OH(resorcinol)	HB	Asn133	1.97
			OH(resorcinol)	HB	Tyr89	2.17
	TCM, Alizarin, 1,2-dihydroxyanthracene-9,10-dione	-6.615 kcal/mol	OH(resorcinol)	HB	Ser99	1.80
			OH(resorcinol)	HB	Ser99	1.73
			O(Quinone)	HB	Tyr89	2.20
			Benzene	π-π	Tyr89	5.19
	SANPDB, (-)- Epicatechin (2 R,3 R)- 2-(3,4-Dihydroxy phenyl)- 3,5,7-chromanetriol	-6.356 kcal/mol	OH(resorcinol)	HB	Leu95	1.88
			OH(resorcinol)	HB	Ser99	1.67
			OH(Oxane)	HB	Asn133	2.22
			OH(Oxane)	HB	Tyr89	1.86
			OH(catechol)	HB	Thr91	2.03
	SANPDB Isoeugenitol 5,7-dihydroxy-2,8-dimethylchromen-4-one	-5.96 kcal/mol	OH(catechol)	HB	Leu95	1.91
			OH(resorcinol)	HB	Ser99	1.99
			CO(Pyranone)	HB	Asn133	2.08
	NENPDB, Gallic acid 3,4,5-trihydroxybenzoic acid	-5.099 kcal/mol	OH(catechol)	HB	Thr94	1.75
			OH(COOH)	HB	Leu95	2.19
			CO(COOH)	HB	Thr91	1.98
			OH(pyrogallol)	HB	Thr91	1.69
	NEANPDB Noreugenin 5,7-dihydroxy-2-methyl chromone	-6.042 kcal/mol	OH(pyrogallol)	HB	Leu95	2.19
			OH(resorcinol)	HB	Thr89	2.09
	EANPDB (-)-mesquitol (2 S,3 R)- 2-(3,4-Dihydroxyphenyl)- 3,7,8-chromanetriol	-5.946 kcal/mol	OH(catechol)	HB	Ser99	2.67
			OH(catechol)	HB	Ser99	1.94
			OH(catechol)	HB	Leu95	2.02
			OH(catechol)	HB	Met93	1.73
			OH(catechol)	HB	Met93	2.05
	EANPDB NA 5,7,3',4'-tetrahydroxyflavanol	-5.689 kcal/mol	OH(Oxane)	HB	Tyr89	2.24
			OH(Oxane)	HB	Thr91	1.95
			OH(resorcinol)	HB	Asp92	2.02

Fig. 3. Interaction pattern of top two hits from SANPDB database with NS1 (**a**) showing the 2D and 3D interaction of top hit 1-NS1 complex (**b**) showing the 2D and 3D interaction of top hit 2-NS1 complex.

Top hits from the traditional Chinese medicine database

In screening of TCM database, we identified two compounds, lathodoratin and alizarin, that exhibited docking scores of − 6.001 kcal/mol and − 6.615 kcal/mol, respectively. Lathodoratin is a phenolic compound isolated from the roots of Lathyrus odoratus, a plant with antitumor and anti-inflammatory activity [71]. Alizarin is an anthraquinone compound obtained from the roots of Rubia cordifolia, a plant with antiviral and antioxidant activity [72]. Lathodoratin is a phenolic compound with a catechol group that can act as a hydrogen bond donor or acceptor, while alizarin is an anthraquinone compound with carbonyl group acting hydrogen bond acceptor and benzene ring as a π-π interaction partner. The distances of the hydrogen bonds ranged from 1.73 to 2.20 Å, while the distance of the π-π interaction was 5.19 Å (Table 1). The Tyr89 was targeted by hydrogen bond by resorcinol hydroxyl group of lathodoratin and Quinone carbonyl oxygen of alizarin. Moreover, lathodoratin formed hydrogen bonds with Met93 and Asn133, while alizarin with Ser99 of NS1-ED via hydroxyl groups of their respective resorcinol or catechol ring. Additionally, alizarin also extended a π-π interaction with Tyr89 of NS1-ED from benzene ring, which could enhance its binding affinity (Fig. 5a & b). These interactions indicate that these compounds could interfere with the NS1-ED binding interface.

Notably, our molecular docking studies reveals the potential of natural compounds from different databases as inhibitors of the influenza NS1-ED protein. The diverse functional groups, including catechol, pyrrolidiniumol, pyrogallol, and chromene, contribute to the binding affinity through specific interactions with key residues. Among all compounds, alizarin, (-)-epicatechin, and haemanthamine showed the lowest docking scores and the most interactions with NS1-ED. These compounds could be promising candidates for the development of novel antiviral agents against influenza A virus. Certainly, we recognize that additional experimental validation is

essential, and further optimization is required to substantiate the efficacy and safety of the findings.

Dynamic stability analysis of top hits and NS1 complexes

Evaluating the dynamic stability of a protein when bound to a ligand is crucial in showcasing the pharmacological effectiveness of that compound. For example, a ligand's firm binding to the protein's active site often correlates with higher pharmacological promise compared to less stable interactions [73]. Demonstrating the stability of these interactions during simulations involves utilizing the RMSD (Root Mean Square Deviation) function within simulation analysis. Therefore, to ascertain the stability of these compounds throughout the simulation, we computed the RMSD for their trajectories over time, as depicted in Figs. 6a-6h. All complexes demonstrated stable dynamics with consistently lower RMSD values. Specifically, the top two compounds sourced from the East Africa (EA) database exhibited notably stable dynamic behaviour. EA-8411902, for instance, rapidly stabilized at 1.3 Å shortly after the 2 ns mark, maintaining high convergence over the entire 200 ns simulation duration with an average RMSD value of 1.4 Å (Fig. 6a). Similarly, the EA-19951545-NS1 complex demonstrated a comparable RMSD value to the previously mentioned compound. This system equilibrated at 2 ns with an RMSD value of 1.3 Å and exhibited consistent stability throughout the simulation, displaying high convergence. The average RMSD for this complex was recorded at 1.3 Å (Fig. 6b). In summary, these top compounds from the EA database displayed remarkable stability and convergence throughout the entire MD simulation period, suggesting their heightened pharmacological activity against the NS1 protein of the influenza virus.

Molecular simulations were conducted on the top hits identified from the North Africa (NA) database, revealing a stable dynamic behaviour. The leading hit, NA-390261, exhibited behaviour similar
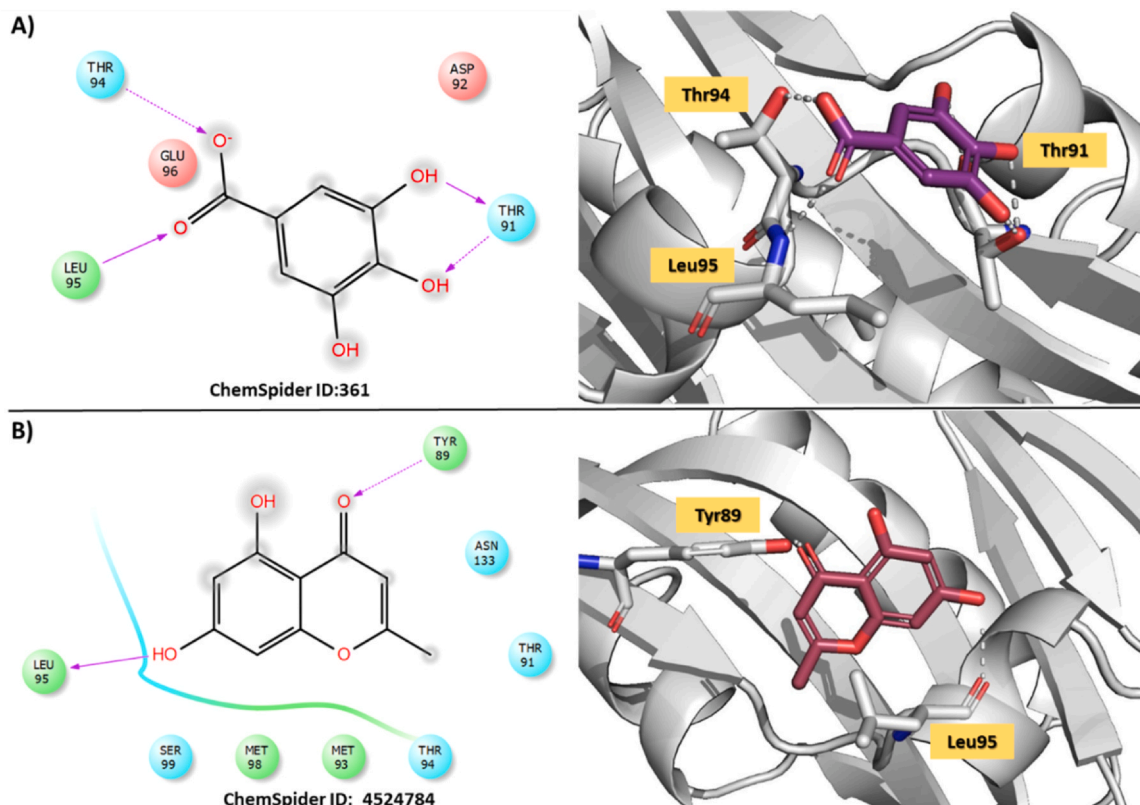
Fig. 4. Interaction pattern of top two hits from NENPDB database with NS1 (**a**) showing the 2D and 3D interaction of top hit 1-NS1 complex (**b**) showing the 2D and 3D interaction of top hit 2-NS1 complex.
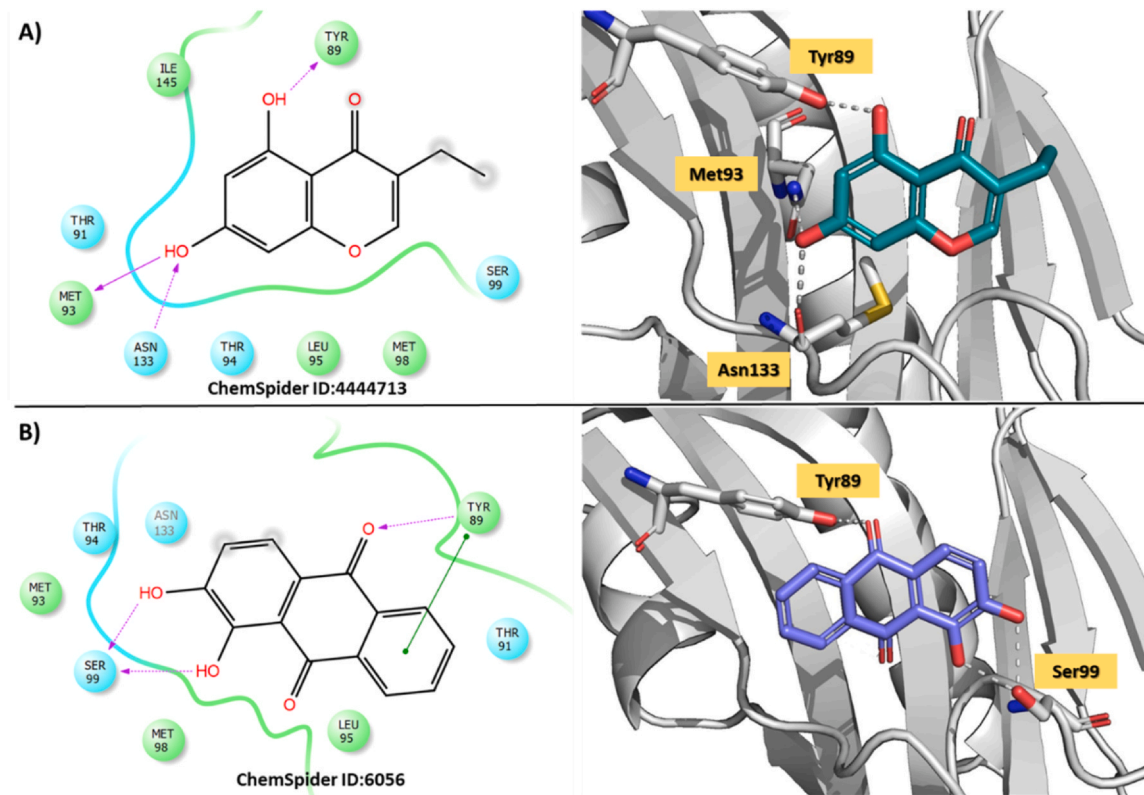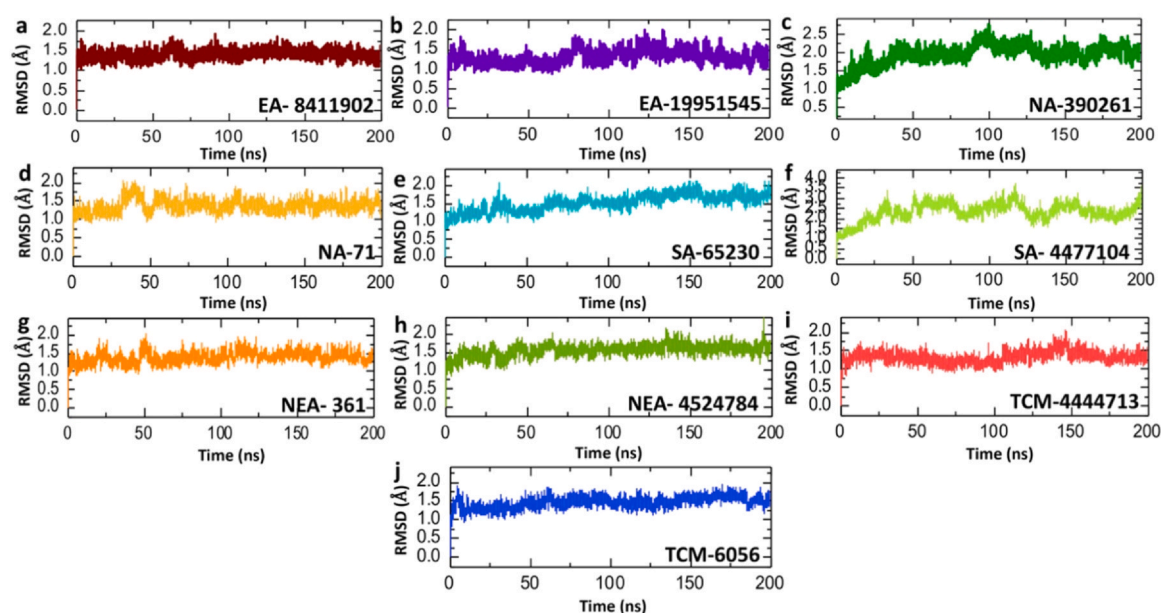

Fig. 5. Interaction pattern of top two hits from TCM database with NS1 (**a**) showing the 2D and 3D interaction of top hit 1-NS1 complex (**b**) showing the 2D and 3D interaction of top hit 2-NS1 complex.

Fig. 6. Stability analysis of top hits compouds-NS1 complexes. (**a, b**) showing the RMSD values of top hits compounds from EA database. (**c, d**) showing the RMSD values of top hits compounds from NA database. (**e, f**) showing the RMSD values of top hits compounds from SA database. (**g, h**) showing the RMSD values of top hits compounds from NEA database. (**i, j**) showing the RMSD values of top hits compounds from TCM database.

to EA compounds but with a slightly higher RMSD value. Initially stabilizing at 1 Å, the complex's RMSD gradually increased, reaching 2 Å at 50 ns. Subsequently, the complex displayed a consistently steady RMSD graph, indicating its stability throughout the simulation. The average RMSD calculated for this complex was 2 Å (Fig. 6**c**). On the other hand, the second top hit, NA-71, showcased an overall stable behaviour, albeit experiencing minor deviations between 25–50 ns. This complex demonstrated high convergence with minimal perturbation in its RMSD value. The average RMSD computed for NA-71 was 1.5 Å (Fig. 6**d**). Comparatively, the second top hit from the NA database displayed a more stable behaviour in terms of RMSD value than the first top hit. The assessment of dynamic stability for these complexes indicates their stable pharmacological behaviour, suggesting potential for improved pharmacological efficacy in in-vitro settings.

Additionally, the stability of the binding of the top hits retrieved from the South Africa (SA) database, namely SA-65230 and SA-4477104, was confirmed through simulation trajectories. As illustrated in Fig. 6**e**, the SA-65230-NS1 complex exhibited consistent and stable dynamic behaviour without significant structural alterations. Despite stabilizing at 1 Å, the Root Mean Square Deviation (RMSD) gradually increased over time, peaking at 1.7 Å, yet maintaining a consistent and linear RMSD pattern, indicating stability throughout the simulation. On the other hand, SA-4477104 displayed minor structural perturbations at various time points. While the system reached equilibrium at 1 Å, the RMSD continued to increase until 50 ns, after which it remained relatively stable with slight fluctuations observed between 100 ns and 150 ns (Fig. 6**f**). Moreover, these compounds demonstrated stable pharmacological properties against NS1 in the all-atoms simulation setup, suggesting their potential efficacy in inhibiting influenza pathogenesis by targeting the NS1 protein.

Moreover, the top hits from the North East Africa (NEA) database, including NEA-361 and NEA-4524784, was assess for their molecular stability. The NEA-361-NS1 complex exhibited a consistent RMSD pattern akin to the previously mentioned complexes. Initially, the system equilibrated within 2 nanoseconds with an RMSD of 1.3 Å, maintaining this stability throughout the simulation period and averaging at 1.3 Å (Fig. 6**g**). Notably, this system displayed a higher level of convergence over the 200 ns simulation duration. Similarly,

NEA-4524784 showed a similar behaviour, demonstrating no significant perturbations during simulation and stabilizing at 1.6 Å. The average RMSD value for this compound was recorded at 1.7 Å, indicating significant convergence throughout the simulation timeframe (Fig. 6**h**). Moreover, TCM-4444713 and TCM6056, the primary compounds identified from Traditional Chinese Medicine (TCM), demonstrated sustained dynamic affinity with the NS1 target. Both of these top-hit compounds formed complexes with NS1 that exhibited a similar pattern, showcasing an average RMSD value of 1.5 Å. These complexes displayed a high level of convergence, showing minimal deviation in the RMSD values (Fig. 6**i & j**). It's evident that all the complexes exhibited lower RMSD values, indicating more stable dynamics when interacting with NS1 due to these novel compounds. Overall, these findings underscore the potential of these compounds as therapeutic options for combating influenza viral pathogenesis, specifically through the inhibition of NS1-TRIM25 interface residues.

Residual fluctuation analysis of top hits and NS1 complexes

The calculation of Root Mean Square Fluctuation (RMSF) stands as a crucial technique in studying protein-drug interactions. It offers valuable insights into protein dynamics, aids in identifying binding sites, validates computational predictions, comprehends drug mechanisms, and supports the process of drug design and refinement [74,75]. By combining RMSF analysis with other computational and experimental methods, our comprehension of protein-drug interactions is amplified, enabling a more rational approach to drug design [76,77]. Hence, in this investigation, we performed RMSF calculations for all the top hits and NS1 complexes to evaluate the fluctuations of individual residues. In the EA database, both EA-8411902 and EA-19951545 exhibited a nearly identical pattern of residue flexibility. Throughout the simulation duration, these compounds displayed lower fluctuation overall, except for a region between 80–90, which showed heightened flexibility. The average RMSF for these complexes was measured at 0.8 Å (Fig. 7**a**). On the other hand, when examining the compound NA-390261-NS1 complex, there was a notable increase in residue flexibility observed in the regions 50–60 and 80–90. In contrast, compound NA-71
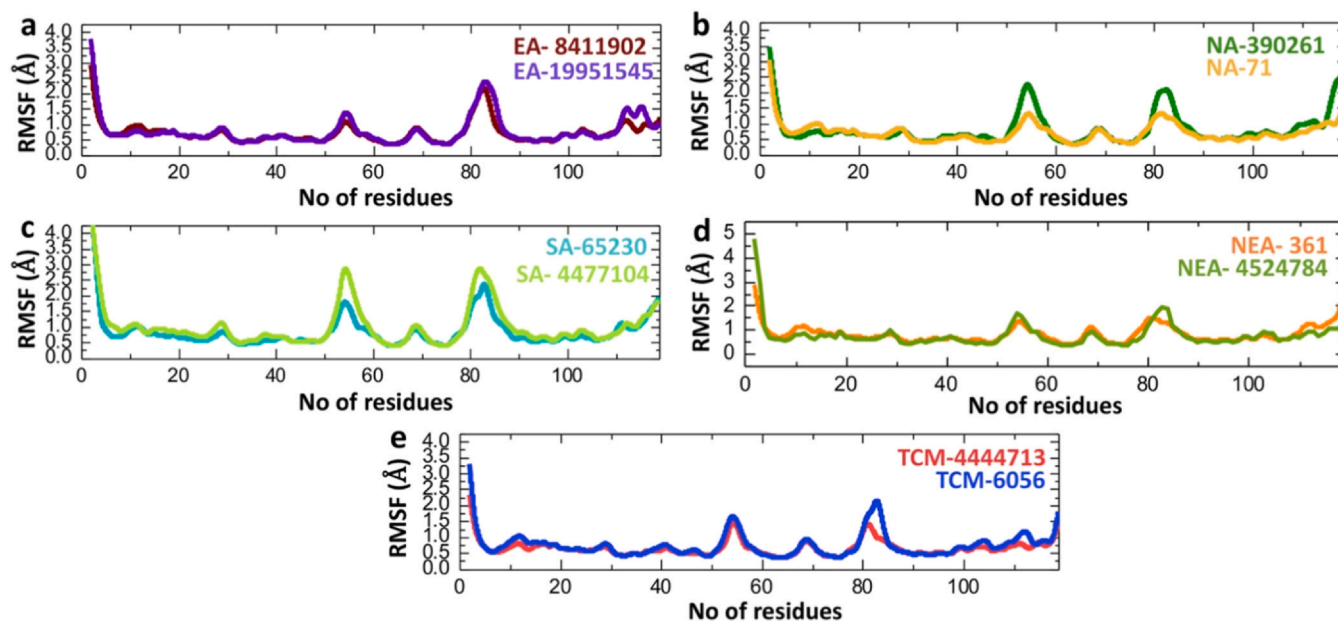
Fig. 7. Fluctuation analysis of top hits-NS1 complexes at residues level. (**a**) represents the fluctuation of top hits compounds from EA database as RMSF. (**b**) represents the fluctuation of top hits compounds from NA database as RMSF. (**c**) represents the fluctuation of top hits compounds from SA database as RMSF. (**d**) represents the fluctuation of top hits compounds from NEA database as RMSF. (**e**) represents the fluctuation of top hits compounds from TCM database as RMSF.

displayed comparatively minor fluctuations in the mentioned regions compared to NA-390261. The average RMSF for the NA database compounds was determined to be 0.7 Å (Fig. 7**b).** The complexes formed by SA database compounds (SA-65230 and SA-4477104) displayed a similar RMSF pattern to that reported in the EA and NA database compounds complexes. However, these SA compounds showed a higher degree of fluctuation in the ranges of 50–60 and 80–90. The average RMSF value for these complexes was approximately 1 Å (Fig. 7**c**). Conversely, the NEA database compounds (NEA-361 and NEA-4524784) exhibited a more stable conformation throughout the simulation period, displaying minimal fluctuation and an average RMSF value of 1 Å (Fig. 7**d**). A comparable outcome was observed for compounds (TCM-4444713 and TCM6056) complexes from the TCM database, with minor variations in the 50–60 and 80–90 range (Fig. 7**e**). This indicates that the interaction of each ligand has a distinct impact on the internal dynamics. Notably, the 80–90 regions encompass the active site residues, suggesting that the movement of this loop plays a role in optimizing the drug's placement within the cavity by expanding the pocket's volume. These specific regions align with loop areas.

Solvent Accessible Surface Area Analysis of top hits and NS1 complexes

SASA analysis, which stands for Solvent Accessible Surface Area analysis, is a computational method extensively utilized in the realms of computational biology and structural bioinformatics. Its primary purpose is to determine the surface area of a molecule that is readily accessible to solvent molecules. This analytical approach finds significant application in studying proteins, DNA, RNA, and various biological macromolecules. It holds immense value in comprehending molecular interactions, identifying ligand binding sites, exploring protein-protein interactions, and predicting the potential behaviour of a molecule concerning its interactions with other molecules or its surrounding environment [78]. Consequently, our study involved calculating the solvent-accessible surface area (SASA) for the top hits and NS1 complexes. Our data revealed minimal fluctuation in SASA across all systems during the simulation period. Specifically, the EA-8411902 and EA-19951545 compounds exhibited an average SASA value of approximately 6900 Å (Fig. 8**a & b**).

Conversely, the NA-390261 and NA-71 compounds displayed slightly higher average SASA values of 7200 Å and 7000 Å, respectively, compared to the EA compounds (Fig. 8**c & d**). Additionally, SASA values of 6900 Å and 7300 Å were observed for the SA-65230 and SA-4477104 compounds, respectively (Fig. 8**e & f**). Similarly, the NEA-361, NEA-4524784, and TCM-4444713 compound-NS1 complexes all showed a recorded SASA value of 6900 Å, while the TCM6056-NS1 complexes resulted in a SASA value of 6800 Å (Fig. 8**g-j**). Overall, the SASA calculations demonstrated relatively consistent values among the EA compounds, with slight variations observed in other compound groups. The NA and SA compounds tended to exhibit slightly higher SASA values, while the NEA and TCM compounds showed comparable SASA values, with minor deviations. The TCM6056-NS1 complexes displayed the lowest SASA among the compounds studied. These findings collectively suggest specific structural and solvent accessibility characteristics among the different compound-NS1 complexes, indicating potential implications for their functional behaviour.

Bonding network analysis of top hits-NS1 complexes in dynamic environment

Hydrogen bonding plays a crucial role in biological systems, facilitating strong intermolecular connections that aid molecular recognition and essential biological processes [72]. Analysis of hydrogen bonds was carried out for all complexes during molecular dynamics (MD) simulations to determine the quantity of hydrogen bonds formed in each frame. As illustrated in Fig. 9, the targeted complexes display a resilient network of hydrogen bonds, highlighting the robust stability of the compounds bound to the protein. Specifically, within the EA database, the average number of hydrogen bonds in each complex was calculated as 60 in EA-8411902 and 63 in EA-19951545 (Fig. 9**a & b**). Furthermore, in the NA database compounds, the average count of hydrogen bonds was computed to be 65 in the NA-390261-NS1 complex and 60 in the NA-71-NS1 complex (Fig. 9**c & d**). Additionally, the average hydrogen bond counts were 56 in the SA-65230-NS1 complex, whereas in the SA-4477104-NS1 complex, they were found to be 55 (Fig. 9**e & f**). Interestingly, a similar hydrogen bond pattern emerged in the NEA-361, NEA-
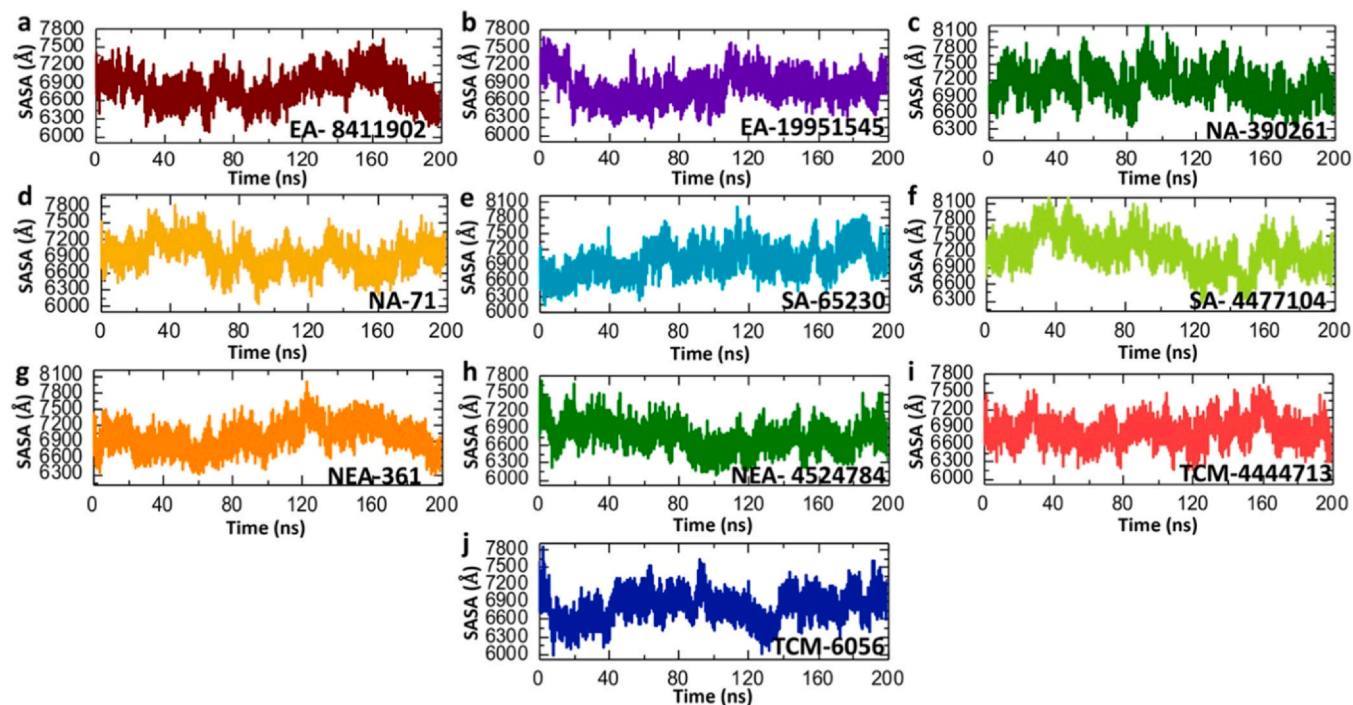
Fig. 8. Surface area analysis of top hits compounds and NS1 protein.

4524784, TCM-4444713, and TCM-6056 compounds-NS1 complexes, averaging 60 hydrogen bonds (Fig. 9**g-j**). The substantial stability observed, as indicated by the earlier discussed RMSD and RMSF data, can be credited to the extensive formation of hydrogen bonds within these systems. This phenomenon might potentially lead to the inhibition of the target protein, consequently reducing the infectivity of the influenza virus.

Dissociation constant analysis

We employed the PRODIGY method to compute the KD values for the complexes formed between the top-hit compounds and NS1. PRODIGY, a specialized web server for forecasting binding affinity in protein-protein and protein-ligand complexes, utilizes fundamental structural characteristics, including interface residue interactions. Its

Fig. 9. Analysis of average hydrogen bonds in top hits-NS1 complexes. **(a, b)** showing the average hydrogen bonds in EA top hits-NS1 complexes. **(c, d)** showing the average 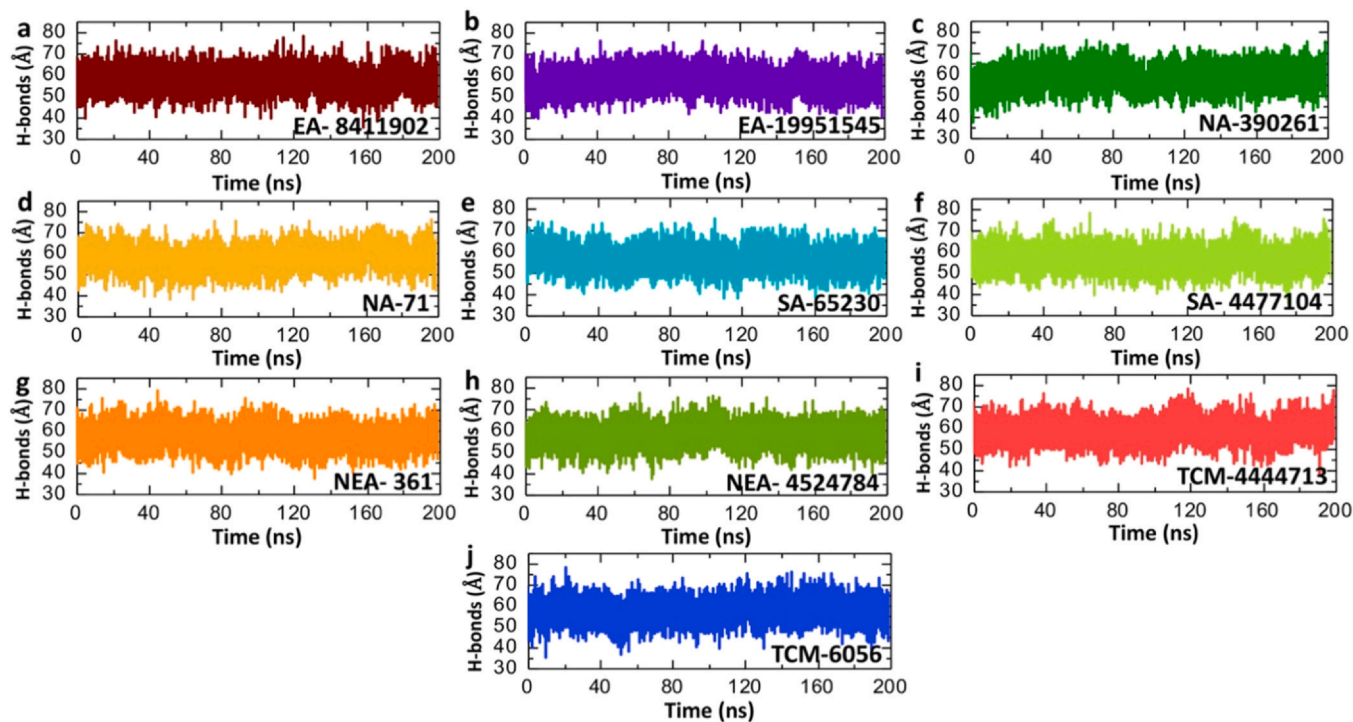hydrogen bonds in NA top hits-NS1 complexes. **(e, f)** showing the average hydrogen bonds in SA top hits-NS1 complexes. **(g, h)** showing the average hydrogen bonds in NEA top hits-NS1 complexes. **(i, j)** showing the average hydrogen bonds in TCM top hits-NS1 complexes.

predictive capabilities exceed those of current predictors, and the PRODIGY-LIG extension, optimized for small ligands, now incorporates atomic contacts for enhanced accuracy [79]. PRODIGY analysis revealed the binding scores of −5.31 kcal/mol for EA-8411902, NEA-4524784, NA-71, TCM-6056, −5.29 kcal/mol for EA-19951545, SA-65230, TCM-4444713, −5.28 kcal/mol for NEA-361, SA-4477104, and −5.10 kcal/mol for NA-390261. The scores demonstrate a robust binding affinity between these compounds and the NS1 protein target. Our results align with several other studies that have also noted a similar range of scores, indicating a notably strong binding affinity within the protein-ligand complexes [53,54].

Lipinski's rule of five analysis for the selected top hits

Assessing drug-like properties involves a qualitative approach used in the development of drugs or drug-like substances, considering various parameters including bioavailability. Furthermore, within the field of pharmacokinetics lies the study of the processes undergone by a chemical after its absorption by a living organism. Predicting pharmacokinetic parameters based on a compound's structure is facilitated by methods such as drug-likeness evaluation and Lipinski's rule of five [80]. As shown in Table 2 all the selected drugs follow Lipinski's rule of five. All the selected drugs have molecular weights less the 500 and the hydrogen bonds acceptors and donors are less than 10 and 5 respectively. The bioavailability score of 0.56 (56%) was recorded for the drugs SA- 4477104 and NEA- 361 however for the rest of the drugs the value of bioavailability was recorded to be 0.55 (55%). The bioavailability score of a drug quantifies the fraction or percentage of the administered dose that reaches systemic circulation in an unchanged form, allowing it to have an active effect on the body. Furthermore, the selected drugs have the log P values less then 5. To sum up, the drugs selected from different databases not only align with the rule of five but also demonstrate pharmacological activity against NS1. This implies that these compounds possess desirable characteristics in terms of molecular weight, bioavailability, and log P values, which could be a significant factor in potential therapeutic applications or drug development efforts.

Analysis of ADMET properties of top hits

The selected compounds' pharmacokinetic properties are outlined in Table 4. In our analysis of absorption attributes, we considered factors like water solubility, Caco-2 permeability, and human intestinal absorption. The extent of drug absorption hinges on water solubility, with higher solubility indicating improved absorption characteristics and greater bioavailability [81]. Compounds EA-8411902, EA-19951545, SA-65230, and TCM-6056 (−3.119, −3.09, −3.124, −3.152) demonstrated significantly greater water solubility compared to other drugs. Caco-2, a human colorectal adenocarcinoma cell line, has been immortalized and is commonly used as a

model for studying the intestinal barrier [82]. Among the top hits compounds, NA-390261 (1.002) and TCM-6056 (1.1) exhibited substantial Caco-2 permeability, whereas EA-8411902 (−0.219) displayed lower permeability. Determining the human intestinal absorption (HIA) rate is crucial for assessing a drug's oral absorption efficacy [83]. Among the chosen candidates, all displayed high rates of intestinal absorption, with TCM-6056 ranking highest at 95.18%, while NEA-361 had the lowest rate at 43.374% for HIA. Additionally, we conducted an analysis on drug distribution characteristics, including the blood-brain barrier and volume of distribution (VD). A VD score below −0.15 suggests a drug is more evenly distributed in plasma rather than in tissues, while a score above 0.45 indicates greater uniformity in tissue distribution. Among the top hits, SA-65230 (−1.298) and NEA-361 (−1.855) have the lowest VD values, indicating a more plasma-oriented distribution. However, SA-65230 (1.346), exhibits the highest VD value, indicating more uniform tissue distribution. Furthermore, regarding the blood-brain barrier (BBB), which restricts substances from entering the central nervous system, five of the selected compounds (NA-390261, SA-4477104, NEA-4524784, TCM-4444713, TCM-6056) can penetrate the BBB (Table 3).

It is widely known that the liver plays a crucial role in breaking down compounds post-drug distribution, employing various enzymatic processes. Among these, cytochrome P450 is an important isoenzyme responsible for the biotransformation and metabolism of drugs [84]. The significance of drug metabolism facilitated by cytochrome P450 stems from concerns regarding both medication toxicity and pharmacological effects [85]. In our analysis, the top hit compounds including SA-4477104, NEA-4524784, TCM-4444713, and TCM-6056 were identified as inhibitors of CYP4501A2. Drug molecules can exit the body through various routes including liver, bile, and kidneys, with the total clearance rate providing crucial information on drug excretion by both liver and kidneys [86]. The organic cation transporter two (OCT2) substrate is pivotal for enhancing renal clearance, yet none of the compounds were found to function as OCT2 substrates. Failure in medication development often stems from toxicity issues, but none of our compounds exhibited toxicities such as skin sensitivity, AMES toxicity, or hepatotoxicity. However, the leading candidate, NA-390261, displayed hepatotoxicity (Table 3).

Binding free energy of top hits compounds and NS1 complexes

Utilizing the MM/GBSA approach, known for its precision in re-evaluating specific binding conformations and energies, we assessed the binding affinities of top-hit compounds with NS1. This method, favored for re-ranking potent inhibitors against their receptors [87,88], revealed total binding free energies of −31.63 kcal/mol and −32.46 kcal/mol for the EA-8411902 and EA-19951545 complexes, respectively. Similarly, the complexes NA-390261, NA-71, SA-65230, and SA-4477104 exhibited recorded values of −32.70 kcal/mol,

Table 2
Lipinski's rule five analysis for all selected top hits.

Drugs ID	Molecular Weight	Hydrogen Acceptors	Hydrogen Donors	Consensus Log P	Lipinski's rule		Bioavailability
					Results	Violation	
EA- 8411902	290.271	6	5	1.5461	Yes	0	0.55
EA-19951545	290.271	6	5	1.6793	Yes	0	0.55
NA-390261	301.342	5	1	1.1867	Yes	0	0.55
NA-71	154.121	3	3	0.796	Yes	0	0.55
SA-65230	290.271	6	5	1.5461	Yes	0	0.55
SA- 4477104	206.197	4	2	1.82104	Yes	0	0.56
NEA- 361	170.12	4	4	0.5016	Yes	0	0.56
NEA- 4524784	192.17	4	2	1.51262	Yes	0	0.55
TCM-4444713	206.197	4	2	1.7666	Yes	0	0.55
TCM-6056	240.214	4	2	1.8732	Yes	0	0.55

Table 3
ADME properties of all selected top hits.

Drugs ID	Water solubility Log S	Caco-2 permeability x 10 − 6	Human Intestinal absorption (%)	VDss (human)	BBB permeability	CYP450 1A2 inhibitor	Renal OCT2 substrate	AMES toxicity	Skin sensitization	Hepato toxicity
EA- 8411902	-3.119	-0.219	66.728	1.116	No	No	No	No	No	No
EA-19951545	-3.09	-0.188	72.864	1.232	No	No	No	No	No	No
NA-390261	-2.035	1.164	87.86	0.733	Yes	No	No	No	No	Yes
NA-71	-2.069	0.49	71.174	-1.298	No	No	No	No	No	No
SA-65230	-3.124	-0.17	69.21	1.346	No	No	No	No	No	No
SA- 4477104	-2.725	1.002	93.126	0.443	Yes	Yes	No	No	No	No
NEA- 361	-2.56	-0.081	43.374	-1.855	No	No	No	No	No	No
NEA- 4524784	-2.697	0.299	93.217	0.649	Yes	Yes	No	No	No	No
TCM-4444713	-2.812	0.917	93.411	0.268	Yes	Yes	No	No	No	No
TCM-6056	-3.152	1.1	95.18	0.192	Yes	Yes	No	No	No	No

Table 4
The binding free energy calculation by MM/GBSA.

MM/GBSA							
Complexes	ΔEvdw	ΔEele	EGB	ESURF	Delta G Gas	Delta G Solv	ΔG total
EA-8411902	-27.72	-6.04	6.20	-4.08	-15.67	4.12	-31.63
EA-19951545	-28.78	-8.45	7.21	-2.44	-18.33	3.77	-32.46
NA-390261	-32.59	-4.54	8.16	-3.73	-25.13	5.43	-32.70
NA-71	-21.60	-9.74	7.00	-4.06	6.14	-16.06	-28.40
SA-65230	-29.82	-3.82	4.42	-3.20	41.00	-45.62	-32.42
SA- 4477104	-28.15	-10.36	8.31	-5.67	-5.51	1.64	-35.87
NEA- 361	-27.63	-10.10	4.70	-4.37	-17.72	4.32	-37.40
NEA-4524784	-23.16	-11.84	7.49	-1.43	-15.00	4.06	-28.94
TCM-4444713	-24.45	-6.64	7.08	-1.88	-17.09	5.21	-25.88
TCM-6056	-23.22	-6.07	4.76	-2.05	-16.15	2.72	-26.57

− 28.40 kcal/mol, − 32.42 kcal/mol, and − 35.87 kcal/mol. Furthermore, the binding free energies for the NEA-361, NEA-4524784, TCM-4444713, and TCM-6056 complexes were determined as − 37.40 kcal/mol, − 28.94 kcal/mol, − 25.88 kcal/mol, and − 26.57 kcal/mol, respectively. Table 4 provides a detailed breakdown of the total binding free energies, van der Waals, and electrostatic energies Table 4.

Conclusion

In conclusion, our in-silico study investigated potential inhibitors targeting the interaction between the influenza A virus non-structural protein 1 (NS1) and the host TRIM25. Utilizing molecular docking and interaction analyses, we focused on compounds sourced from diverse natural product databases, including Traditional Chinese Medicine, African Natural Product Database, South African Natural Product Database, and East African Natural Product Database. Compounds such as (-)-mesquitol, 5,7,3′,4′-tetrahydroxyflavanol, haemanthamine, protocatechuic acid, (-)-epicatechin, isoeugenitol, gallic acid, 5,7-dihydroxy-2-methylchromone, lathodoratin, and alizarin exhibited strong binding affinity to NS1-ED, forming crucial hydrogen bonds that inhibit NS1-TRIM25 binding. Dynamic Stability Analysis indicates stable dynamics (low RMSD), Residual Fluctuation Analysis shows minor conformational fluctuations, SASA Analysis reveals consistent values in structural characteristics, and Hydrogen Bonding Analysis demonstrates a resilient network, collectively suggesting potential pharmacological activity in NS1-bound compounds. Dissociation Constant and binding free energies calculation reinforces the compounds' potential as antiviral agents by indicating strong binding affinity. Lipinski's Rule of Five Analysis confirms the compounds' adherence to desirable drug-like properties, including molecular weight, bioavailability, and log P values. ADMET Properties Analysis further supports

the potential application of these compounds, revealing favourable pharmacokinetic properties such as water solubility, permeability, and intestinal absorption. Some compounds also exhibit inhibitory effects on CYP4501A2, a key enzyme in drug metabolism. These compounds demonstrate stability, favourable characteristics resembling drug properties, and minimal toxicity, indicating their appropriateness for in-depth exploration (in-vitro and in-vivo validation) and potential development as therapeutic agents against influenza A.

Declaration of Competing Interest

The authors declare that they have no known competing financial interests or personal relationships that could have appeared to influence the work reported in this paper.

References

[1] Jiang C, Yao X, Zhao Y, Wu J, Huang P, Pan C, et al. Comparative review of respiratory diseases caused by coronaviruses and influenza A viruses during epidemic season. Microbes Infect 2020;22(6-7):236–44.
[2] Organization W.H. Sex, gender and influenza: World Health Organization; 2010.
[3] Macias AE, McElhaney JE, Chaves SS, Nealon J, Nunes MC, Samson SI, et al. The disease burden of influenza beyond respiratory illness. Vaccine 2021;39:A6–14.

[4] Aglipay M, Birken CS, Parkin PC, Loeb MB, Thorpe K, Chen Y, et al. Effect of high-dose vs standard-dose wintertime vitamin D supplementation on viral upper respiratory tract infections in young healthy children. Jama 2017;318(3):245–54.

[5] Kumar B, Asha K, Khanna M, Ronsard L, Meseko CA, Sanicas M. The emerging influenza virus threat: status and new prospects for its therapy and control. Arch Virol 2018;163:831–44.

[6] James S., Sargent T.C. The economic impact of an influenza pandemic: Department of Finance; 2007.

[7] Hsu AC-Y. Influenza virus: a master tactician in innate immune evasion and novel therapeutic interventions. Front Immunol 2018;9:743.

[8] Reikine S, Nguyen JB, Modis Y. Pattern recognition and signaling mechanisms of RIG-I and MDA5. Front Immunol 2014;5:342.

[9] Pichlmair A, Schulz O, Tan CP, Naslund TI, Liljeström P, Weber F, et al. RIG-I-mediated antiviral responses to single-stranded RNA bearing 5′-phosphates. Science 2006;314(5801):997–1001.

[10] Sun X, Xian H, Tian S, Sun T, Qin Y, Zhang S, et al. A hierarchical mechanism of RIG-I ubiquitination provides sensitivity, robustness and synergy in antiviral immune responses. Sci Rep 2016;6(1):29263.

[11] Kowalinski E, Lunardi T, McCarthy AA, Louber J, Brunel J, Grigorov B, et al. Structural basis for the activation of innate immune pattern-recognition receptor RIG-I by viral RNA. Cell 2011;147(2):423–35.

[12] Chiang JJ, Davis ME, Gack MU. Regulation of RIG-I-like receptor signaling by host and viral proteins. Cytokine Growth Factor Rev 2014;25(5):491–505.

[13] Chan YK, Gack MU. RIG-I-like receptor regulation in virus infection and immunity. Curr Opin Virol 2015;12:7–14.

[14] Kim M-J, Hwang S-Y, Imaizumi T, Yoo J-Y. Negative feedback regulation of RIG-I-mediated antiviral signaling by interferon-induced ISG15 conjugation. J Virol 2008;82(3):1474–83.

[15] Cadena C., Ahmad S., Xavier A., Willemsen J., Park S., Park J.W., et al. Ubiquitin-dependent and-independent roles of E3 ligase RIPLET in innate immunity. Cell. 2019;177(5):1187–1200. e16.

[16] Hayman TJ, Hsu AC, Kolesnik TB, Dagley LF, Willemsen J, Tate MD, et al. RIPLET, and not TRIM25, is required for endogenous RIG-I-dependent antiviral responses. Immunol Cell Biol 2019;97(9):840–52.

[17] Choudhury NR, Trus I, Heikel G, Wolczyk M, Szymanski J, Bolembach A, et al. TRIM25 inhibits influenza A virus infection, destabilizes viral mRNA, but is redundant for activating the RIG-I pathway. Nucleic Acids Res 2022;50(12):7097–114.

[18] Zinzula L, Tramontano E. Strategies of highly pathogenic RNA viruses to block dsRNA detection by RIG-I-like receptors: hide, mask, hit. Antivir Res 2013;100(3):615–35.

[19] Liu Y, Olagnier D, Lin R. Host and viral modulation of RIG-I-mediated antiviral immunity. Front Immunol 2017;7:662.

[20] Marc D. Influenza virus non-structural protein NS1: interferon antagonism and beyond. J Gen Virol 2014;95(12):2594–611.

[21] Carrillo B, Choi J-M, Bornholdt ZA, Sankaran B, Rice AP, Prasad BV. The influenza A virus protein NS1 displays structural polymorphism. J Virol 2014;88(8):4113–22.

[22] Hale BG. Conformational plasticity of the influenza A virus NS1 protein. J Gen Virol 2014;95(10):2099–105.

[23] Cheng A, Wong SM, Yuan YA. Structural basis for dsRNA recognition by NS1 protein of influenza A virus. Cell Res 2009;19(2):187–95.

[24] Koliopoulos MG, Lethier M, van der Veen AG, Haubrich K, Hennig J, Kowalinski E, et al. Molecular mechanism of influenza A NS1-mediated TRIM25 recognition and inhibition. Nat Commun 2018;9(1):1820.

[25] Kim HJ, Jeong MS, Jang SB. Structure and activities of the NS1 influenza protein and progress in the development of small-molecule drugs. Int J Mol Sci 2021;22(8):4242.

[26] Rosário-Ferreira N, Preto AJ, Melo R, Moreira IS, Brito RM. The central role of non-structural protein 1 (NS1) in influenza biology and infection. Int J Mol Sci 2020;21(4):1511.

[27] Chassagne F, Cabanac G, Hubert G, David B, Marti G. The landscape of natural product diversity and their pharmacological relevance from a focus on the Dictionary of Natural Products®. Phytochem Rev 2019;18:601–22.

[28] Shahrajabian MH, Sun W, Cheng Q. The importance of flavonoids and phytochemicals of medicinal plants with antiviral activities. Mini-Rev Org Chem 2022;19(3):293–318.

[29] Mehrbod P, Safari H, Mollai Z, Fotouhi F, Mirfakhraei Y, Entezari H, et al. Potential antiviral effects of some native Iranian medicinal plants extracts and fractions against influenza A virus. BMC Complement Med Ther 2021;21(1):1–12.

[30] Zhang ZJ, Morris-Natschke SL, Cheng YY, Lee KH, Li RT. Development of anti-influenza agents from natural products. Med Res Rev 2020;40(6):2290–338.

[31] LOPES JPPB. Influenza A Virus: From Infection to Prevention. Long-term Effects of an Early Life IAV Infection in vivo and Optimization of the Live Attenuated Influenza A Vaccine Backbone Using Mouse Models.

[32] Xia S. High throughput screening of inhibitors for influenza protein NS1. 2009.

[33] Cunha AE, Loureiro RJ, Simões CJ, Brito RM. Unveiling new druggable pockets in influenza non-structural protein 1: NS1–host interactions as antiviral targets for flu. Int J Mol Sci 2023;24(3):2977.

[34] Guedes IA, de Magalhães CS, Dardenne LE. Receptor–ligand molecular docking. Biophys Rev 2014;6:75–87.

[35] Morris CJ, Corte DD. Using molecular docking and molecular dynamics to investigate protein-ligand interactions. Mod Phys Lett B 2021;35(08):2130002.

[36] Bera I, Payghan PV. Use of molecular dynamics simulations in structure-based drug discovery. Curr Pharm Des 2019;25(31):3339–49.

[37] Sorokina M, Steinbeck C. Review on natural products databases: where to find data in 2020. J Chemin- 2020;12(1):20.

[38] Lemmon G, Meiler J. Towards ligand docking including explicit interface water molecules. PloS One 2013;8(6):e67536.

[39] Zhang S, Krumberger M, Morris MA, Parrocha CMT, Kreutzer AG, Nowick JS. Structure-based drug design of an inhibitor of the SARS-CoV-2 (COVID-19) main protease using free software: A tutorial for students and scientists. Eur J Med Chem 2021;218:113390.

[40] Sayaf AM, Khalid SU, Hameed JA, Alshammari A, Khan A, Mohammad A, et al. Exploring the natural products chemical space through a molecular search to discover potential inhibitors that target the hypoxia-inducible factor (HIF) prolyl hydroxylase domain (PHD). Front Pharmacol 2023;14.

[41] Ravindranath PA, Forli S, Goodsell DS, Olson AJ, Sanner MF. AutoDockFR: advances in protein-ligand docking with explicitly specified binding site flexibility. PLoS Comput Biol 2015;11(12):e1004586.

[42] Khan A, Randhawa AW, Balouch AR, Mukhtar N, Sayaf AM, Suleman M, et al. Blocking key mutated hotspot residues in the RBD of the omicron variant (B. 1.1. 529) with medicinal compounds to disrupt the RBD-hACE2 complex using molecular screening and simulation approaches. RSC Adv 2022;12(12):7318–27.

[43] Case DA, Cheatham III TE, Darden T, Gohlke H, Luo R, Merz Jr KM, et al. The Amber biomolecular simulation programs. J Comput Chem 2005;26(16):1668–88.

[44] Salomon-Ferrer R, Case DA, Walker RC. An overview of the Amber biomolecular simulation package. Wiley Interdisciplinary Reviews. Comput Mol Sci 2013;3(2):198–210.

[45] Toukmaji A, Sagui C, Board J, Darden T. Efficient particle-mesh Ewald based approach to fixed and induced dipolar interactions. J Chem Phys 2000;113(24):10913–27.

[46] Fyta M. Atomistic methods. Computational Approaches in Physics: Morgan & Claypool Publishers; 2016.

[47] Salomon-Ferrer R, Gotz AW, Poole D, Le Grand S, Walker RC. Routine microsecond molecular dynamics simulations with AMBER on GPUs. 2. Explicit solvent particle mesh Ewald. J Chem Theory Comput 2013;9(9):3878–88.

[48] Roe DR, Cheatham TE. PTRAJ and CPPTRAJ: software for processing and analysis of molecular dynamics trajectory data. J Chem Theory Comput 2013;9(7):3084–95.

[49] Maiorov VN, Crippen GM. Significance of root-mean-square deviation in comparing three-dimensional structures of globular proteins. J Mol Biol 1994;235(2):625–34.

[50] Cooper A. Thermodynamic fluctuations in protein molecules. Proc Natl Acad Sci 1976;73(8):2740–1.

[51] Lobanov MY, Bogatyreva N, Galzitskaya O. Radius of gyration as an indicator of protein structure compactness. Mol Biol 2008;42:623–8.

[52] Sayaf AM, Ahmad H, Aslam MA, Ghani SA, Bano S, Yousafi Q, et al. Pharmacotherapeutic potential of natural products to target the SARS-CoV-2 PLpro using molecular screening and simulation approaches. Appl Biochem Biotechnol 2023:1–20.

[53] Khan A, Adil S, Qudsia HA, Waheed Y, Alshabrmi FM, Wei D-Q. Structure-based design of promising natural products to inhibit thymidylate kinase from Monkeypox virus and validation using free energy calculations. Comput Biol Med 2023;158:106797.

[54] Suleman M, Murtaza A, Khan H, Rashid F, Alshammari A, Ali L, et al. The XBB. 1.5 slightly increase the binding affinity for host receptor ACE2 and exhibit strongest immune escaping features: molecular modeling and free energy calculation. Front Mol Biosci 2023;10:1153046.

[55] Suleman M, Yousafi Q, Ali J, Ali SS, Hussain Z, Ali S, et al. Bioinformatics analysis of the differences in the binding profile of the wild-type and mutants of the SARS-CoV-2 spike protein variants with the ACE2 receptor. Comput Biol Med 2021;138:104936.

[56] Khan A, Umbreen S, Hameed A, Fatima R, Zahoor U, Babar Z, et al. In silico mutagenesis-based remodelling of SARS-CoV-1 peptide (ATLQAIAS) to inhibit SARS-CoV-2: structural-dynamics and free energy calculations. Interdiscip Sci: Comput Life Sci 2021;13:521–34.

[57] Pollastri MP. Overview on the rule of five. Curr Protoc Pharmacol 2010;49(1). 9.12.

[58] Daina A, Michielin O, Zoete V. SwissADME: a free web tool to evaluate pharmacokinetics, drug-likeness and medicinal chemistry friendliness of small molecules. Sci Rep 2017;7(1):42717.

[59] Li AP. Screening for human ADME/Tox drug properties in drug discovery. Drug Discov Today 2001;6(7):357–66.

[60] Pires D., Blundell T., Ascher pkC.S.M.D. Predicting small-molecule pharmacokinetic and toxicity properties using graph-based signatures., 2015, 58. DOI: https://doi org/101021/acs jmedchem 5b00104.4066–72.

[61] Li B, Ma C, Zhao X, Hu Z, Du T, Xu X, et al. YaTCM: yet another traditional Chinese medicine database for drug discovery. Comput Struct Biotechnol J 2018;16:600–10.

[62] Ntie-Kang F, Telukunta KK, Fobofou SA, Chukwudi Osamor V, Egieyeh SA, Valli M, et al. Computational applications in secondary metabolite discovery (CAiSMD): an online workshop. BioMed Cent 2021;13:64.

[63] Prabha DS, Dahms H-U, Malliga P. Pharmacological potentials of phenolic compounds from Prosopis spp.-a. J Coast Life Med 2014;2:918–24.

[64] Ngadjui BVT, Abegaz BM. The chemistry and pharmacology of the genus Dorstenia (Moraceae). Stud Nat Prod Chem 2003;29:761–805.

[65] Viladomat F, Bastida J, Codina C, Nair J, Campbell W. Alkaloids of the south african Amaryllidaceae. Recent Res Dev Phytochem 1997;1:131–71.

[66] Abcha I, Ben Haj Said L, Salmieri S, Criado P, Neffati M, Lacroix M. Optimization of extraction parameters, characterization and assessment of bioactive properties of Ziziphus lotus fruit pulp for nutraceutical potential. Eur Food Res Technol 2021;247(9):2193–209.

[67] Bernatova I. Biological activities of (−)-epicatechin and (−)-epicatechin-containing foods: Focus on cardiovascular and neuropsychological health. Biotechnol Adv 2018;36(3):666–81.

[68] Fındık E, Ceylan M, Elmastaş M. Isoeugenol-based novel potent antioxidants: Synthesis and reactivity. Eur J Med Chem 2011;46(9):4618–24.

[69] Bag A, Bhattacharyya SK, Chattopadhyay RR. The development of Terminalia chebula Retz.(Combretaceae) in clinical research. Asian Pac J Trop Biomed 2013;3(3):244–52.

[70] Brown RT, Blackstock WP, Chapple CL. Isolation of 5, 7-dihydroxy-2-methylchromone and its 7-O-glycosides from Adina rubescens. J Chem Soc, Perkin Trans 1 1975(18):1776–8.

[71] Evuen UF, Okolie NP, Apiamu A. Evaluation of the mineral composition, phytochemical and proximate constituents of three culinary spices in Nigeria: a comparative study. Sci Rep 2022;12(1):20705.

[72] Ali A, Aslam M, Chaudhary SS. A Review A Review on Pharmacognostic and Therapeutic Uses of Rubia cordifolia. J Drug Deliv Ther 2020;10(6):195–202.

[73] Karplus M, Kuriyan J. Molecular dynamics and protein function. Proc Natl Acad Sci 2005;102(19):6679–85.

[74] Fatriansyah JF, Boanerges AG, Kurnianto SR, Pradana AF, Surip SN. Molecular dynamics simulation of ligands from Anredera cordifolia (Binahong) to the main protease (M pro) of SARS-CoV-2. J Trop Med 2022;2022.

[75] Ghufran M, Khan HA, Ullah M, Ghufran S, Ayaz M, Siddiq M, et al. In silico strategies for designing of peptide inhibitors of oncogenic K-ras G12V mutant: Inhibiting cancer growth and proliferation. Cancers 2022;14(19):4884.

[76] Rashid F, Suleman M, Shah A, Dzakah EE, Chen S, Wang H, et al. Structural analysis on the severe acute respiratory syndrome coronavirus 2 non-structural protein 13 mutants revealed altered bonding network with TANK binding kinase 1 to evade host immune system. Front Microbiol 2021;12:789062.

[77] Shah A, Rehmat S, Aslam I, Suleman M, Batool F, Aziz A, et al. Comparative mutational analysis of SARS-CoV-2 isolates from Pakistan and structural-functional implications using computational modelling and simulation approaches. Comput Biol Med 2022;141:105170.

[78] Marsh JA, Teichmann SA. Relative solvent accessible surface area predicts protein conformational changes upon binding. Structure 2011;19(6):859–67.

[79] Vangone A, Schaarschmidt J, Koukos P, Geng C, Citro N, Trellet ME, et al. Large-scale prediction of binding affinity in protein–small ligand complexes: The PRODIGY-LIG web server. Bioinformatics 2019;35(9):1585–7.

[80] Lipinski CA. Lead-and drug-like compounds: the rule-of-five revolution. Drug Discov Today: Technol 2004;1(4):337–41.

[81] Xu W, Ling P, Zhang T. Polymeric micelles, a promising drug delivery system to enhance bioavailability of poorly water-soluble drugs. J Drug Deliv 2013;2013.

[82] Lea T. Caco-2 cell line. Impact Food Bioact Health: Vitr Models 2015:103–11.

[83] Arora D., Khurana B. Computer-Aided Biopharmaceutical Characterization: Gastrointestinal Absorption Simulation and In Silico Computational Modeling. Computer Aided Pharmaceutics and Drug Delivery: An Application Guide for Students and Researchers of Pharmaceutical Sciences: Springer; 2022. 1st ed. p. 189–215.

[84] Cresteil T, Monsarrat B, Alvinerie P, Tréluyer JM, Vieira I, Wright M. Taxol metabolism by human liver microsomes: identification of cytochrome P450 isozymes involved in its biotransformation. Cancer Res 1994;54(2):386–92.

[85] Ogu CC, Maxa JL, editors. Drug interactions due to cytochrome P450. Baylor University Medical Center Proceedings; 2000;13(4):421–3 Taylor & Francis.

[86] Dowd F.J., Johnson B., Mariotti A. Pharmacology and therapeutics for dentistry-E-book: Elsevier Health Sciences; 7th ed. elsevier; 2016.

[87] Wang E, Sun H, Wang J, Wang Z, Liu H, Zhang JZ, et al. End-point binding free energy calculation with MM/PBSA and MM/GBSA: strategies and applications in drug design. Chem Rev 2019;119(16):9478–508.

[88] Khan A, Zia T, Suleman M, Khan T, Ali SS, Abbasi AA, et al. Higher infectivity of the SARS-CoV-2 new variants is associated with K417N/T, E484K, and N501Y mutants: an insight from structural data. J Cell Physiol 2021;236(10):7045–57.